

Magnetoresistance relaxation steps originating from dynamic spin-orbital interactions in $\text{Ca}_3\text{Ru}_2\text{O}_7$ Hao-Yu Niu ^{1,*}, Xiong He ^{1,*}, Zhuo Zeng,¹ Yu-Jie Song,¹ De-Quan Jiang,¹ Hao Huang ¹, You-Yuan Liang ¹,
Li-Xia Xiao,² Zhong-Wen Ouyang,^{1,†} and Zheng-Cai Xia ^{1,‡}¹Wuhan National High Magnetic Field Center and School of Physics of Huazhong University of Science and Technology, Wuhan 430074, China²Department of Physics of Wenhua College, Wuhan 430074, China

(Received 14 April 2022; revised 3 November 2022; accepted 7 November 2022; published 16 November 2022)

The in-plane magnetoresistance and magnetostriction of $\text{Ca}_3\text{Ru}_2\text{O}_7$ single crystals were investigated under pulsed magnetic field. Field-induced resistance steps and structural change were observed for specific field directions and far below the metal-to-insulator transition temperature $T_{\text{MI}} = 48$ K, which were not observed under static magnetic field. Especially, the resistance steps were only observed in the field-descending branch, indicating the relaxation properties, and no magnetization steps were observed. These results unveil the existence of instantaneous interactions among different degrees of freedom in $\text{Ca}_3\text{Ru}_2\text{O}_7$, which are observable under pulsed magnetic field thanks to its fast field sweep rate. Based on the orbital states of $\text{Ca}_3\text{Ru}_2\text{O}_7$ and the Kugel-Khomskii model, we propose that the resistance steps and the structural change are related to a dynamic spin-orbital interaction, and this interaction can be strongly suppressed by the magnetocrystalline anisotropy.

DOI: [10.1103/PhysRevB.106.174415](https://doi.org/10.1103/PhysRevB.106.174415)**I. INTRODUCTION**

The interplay between spin, charge, orbital, and lattice degrees of freedom has attracted enormous interest due to the rich physical phenomena, which ceaselessly improve current theoretical research and facilitate future applications. To be specific, the spin-spin interaction can give rise to magnetic ordering, and the spin-charge interaction can lead to the giant magnetoresistance (GMR) effect [1]. The spin-orbital interaction can cause the well-known relativistic spin-orbital coupling (SOC) which is the primary source of the magnetocrystalline anisotropy, and the Kugel-Khomskii interaction which results in the orbital ordering (OO). According to the Kugel-Khomskii model, whether the occupied orbitals at neighboring sites are the same or not is strongly influenced by whether the neighboring spins are aligned in the same or opposite directions [2,3]. The orbital-lattice interaction can also generate the OO via the cooperative Jahn-Teller (JT) effect [4], etc. Interestingly, exotic electromagnetic states can be realized through the cooperation and competition among these interactions.

Ruddlesden-Popper-type ruthenates $(\text{Sr}_{1-x}\text{Ca}_x)_{n+1}\text{Ru}_n\text{O}_{3n+1}$ are perfect materials for studying the above topic. Since the $4d$ orbitals of Ru are more extended than $3d$ orbitals, the interplay of spin, charge, orbital, and lattice degrees of freedom in ruthenates is thus more complicated than that in $3d$ transition metal oxides, resulting in a rich variety of exotic properties. As the number of

perovskite layers increases, the transformation of properties of these compounds becomes increasingly fascinating [5–10]. $\text{Ca}_3\text{Ru}_2\text{O}_7$ is a prototype of this family; it lies in the paramagnetic (PM) phase with metallic behavior when $T > 56$ K [11–13]. At $T_N = 56$ K, as shown in Fig. 1, it undergoes a paramagnetic-antiferromagnetic (PM-AFM) transition, in which the ferromagnetic (FM) bilayers stack antiferromagnetically along the c axis with the magnetic moments aligned along the a axis (AFM- a), and the metallic behavior remains. At $T_{\text{MI}} = 48$ K, the b axis becomes the magnetic easy axis (AFM- b), which is accompanied with a metal-to-insulator transition (MIT), in which the shortening of the c axis and enlarging of both the a axis and the b axis directly lead to the lattice distortion [11]. Recent work has suggested that the MIT results from a partial gap opening near the Fermi surface [14]. Especially, the four d electrons of the Ru^{4+} ion occupy the triply degenerate t_{2g} orbitals in a low-spin state with a net spin of $S = 1$, leading to the t_{2g} active OO [15,16]. In contrast to the e_g active OO, in which the JT effect is much stronger due to the related d orbitals directly pointing to ligands [17], t_{2g} active OO shows a relatively weaker JT effect, which can compete with the spin-orbital coupling [18,19]. Moreover, using mesoscale optical second-harmonic imaging and atomic-resolution scanning transmission electron microscopy, Lei *et al.* confirmed the existence of a quasi-two-dimensional polar domain in $\text{Ca}_3\text{Ru}_2\text{O}_7$ [20]. Despite the extensive studies on this correlated electronic system [11–16,20–35], the dynamic characteristics of the interactions in this system have been less studied, and intriguing dynamics-induced phenomena may also be expected.

In this paper, we have systematically investigated the electrical transport and magnetic properties of $\text{Ca}_3\text{Ru}_2\text{O}_7$ single

*These authors contributed equally to this work.

†Corresponding author: zwouyang@mail.hust.edu.cn‡Corresponding author: xia9020@hust.edu.cn

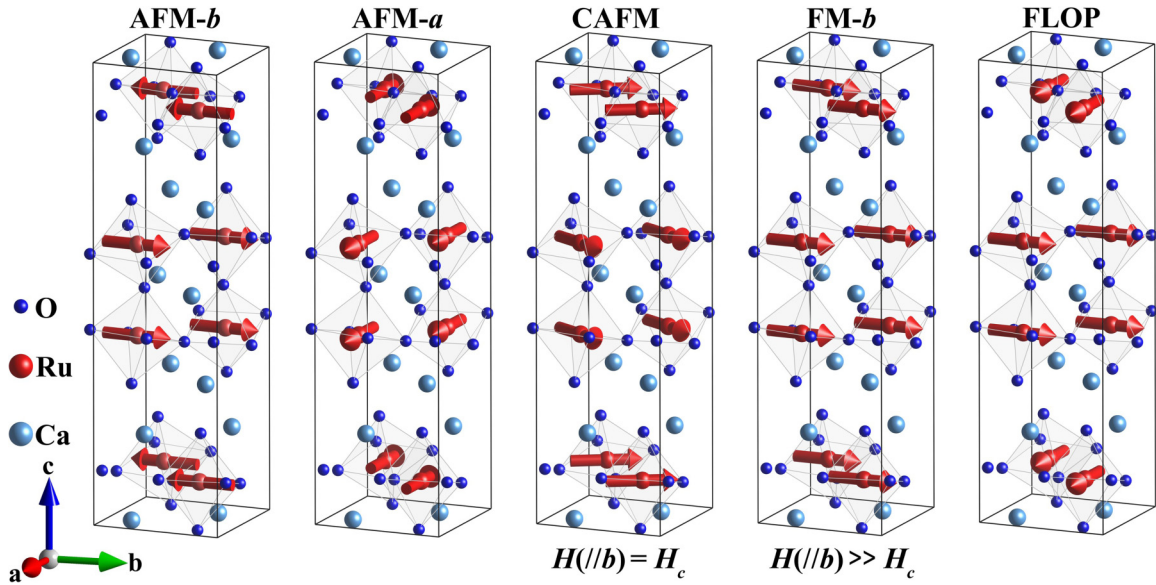


FIG. 1. Crystal and magnetic structures of $\text{Ca}_3\text{Ru}_2\text{O}_7$. The red arrows through the Ru atoms represent the orientations of the spins. For $H \parallel b$ and $T < 40$ K, the spin configuration turns from the AFM- b to the CAFM one at $H = H_c$, and the FM- b state can be realized when $H \gg H_c$.

crystals; unusual in-plane resistance steps were observed under pulsed magnetic field, which exhibit significant dynamic properties. To understand this phenomenon, magnetostriction measurements and density functional theory (DFT) calculations were carried out. We suggest that the observed steps are related to the orbital degrees of freedom and might result from the establishment of metastable states that originates from transient Kugel-Khomskii-type spin-orbital interactions.

II. METHODS

$\text{Ca}_3\text{Ru}_2\text{O}_7$ single crystals were grown using the flux method [28]. Crystallographic directions were determined by Laue x-ray diffraction measurements. The static-field magnetization measurements were performed using a superconducting quantum interference device (SQUID), and the static-field magnetoresistance was studied by the standard four-probe technique with a physical property measurement system (PPMS). Pulsed-field magnetization, magnetoresistance, and magnetostriction measurements and DFT calculations were performed at Wuhan National High Magnetic Field Center. Resistance-type strain gauges were used for the magnetostriction measurements. DFT calculations were performed using the Vienna *ab initio* simulation package (VASP) [36] with the Perdew-Burke-Ernzerhof (PBE) [37,38] exchange correlation functional within the projector-augmented wave (PAW) [39] method. We chose $3s^2, 3p^6, 4s^2$ (Ca); $5s^2, 4d^6$ (Ru); and $2s^2, 2p^4$ (O) as the electronic configurations, and a 500 eV energy cutoff was used. All the magnetic orders were realized with electron correlations in Ru-4d electrons ($U_{\text{eff}} = 1.2$ eV) in a $7 \times 7 \times 5$ Monkhorst-Pack k -point mesh with SOC.

III. RESULTS AND DISCUSSION

The magnetic field dependence of magnetization and in-plane resistivity are illustrated in Fig. 2; the field-induced

transition of ρ_b is in good agreement with the magnetization behavior, signifying the strong spin-charge coupling in this system. For $H \parallel b$, as depicted in Fig. 2(a), $\text{Ca}_3\text{Ru}_2\text{O}_7$ undergoes a first-order metamagnetic transition occurring at H_c ($H_c \approx 6.3$ T at 2 K) with a typical hysteresis loop when $T < 40$ K, in which the spin configuration turns from the AFM- b one to the canted AFM (CAFM) one and the fully FM state can be realized at the high-field region (see Fig. 1) [12]. As the temperature increases, the hysteresis loop becomes narrow, and the critical field H_c of the phase transition gradually decreases; the first-order metamagnetic transition turns into a second-order one above T_{MI} . For $H \parallel a$, $\text{Ca}_3\text{Ru}_2\text{O}_7$ goes through a second-order phase transition below T_{MI} . Intuitively, the magnetization and magnetoresistance curves for $H \parallel [110]$ might be regarded as a combination of those for $H \parallel a$ and $H \parallel b$; when $T < 30$ K, the behavior is dominated by the $H \parallel b$ component, and when $T > 30$ K, the $H \parallel a$ component is primary. As displayed in Fig. 2(e), it is clear that the magnetic moments at 7 T become small due to the fact that $[110]$ is not the easy axis of $\text{Ca}_3\text{Ru}_2\text{O}_7$, and the magnetic moments are not fully polarized. The above anisotropic properties of magnetization and resistivity indicate the presence of strong SOC in this system; the DFT results also manifest the significance of SOC and are shown in Fig. S3(b) of the Supplemental Material [40].

The pulsed magnetic field has a fast field sweep rate, which is an excellent tool to reveal the dynamic properties of $\text{Ca}_3\text{Ru}_2\text{O}_7$. Since the magnetic and magnetoresistance behaviors for $H \parallel a$ and $H \parallel b$ are different, magnetic phase transitions tuned by the in-plane orientation angle of the magnetic field can be expected. To investigate the potential dynamic properties in $\text{Ca}_3\text{Ru}_2\text{O}_7$, in-plane angle-dependent magnetoresistance measurements under pulsed magnetic field were performed; the results are shown in Fig. 3. θ is selected from several different angles ranging from 0° ($H \parallel b$) to 90° ($H \parallel a$); a multistep change in ρ_b was observed in the field-descending branch for some specific field directions. As θ increases, the

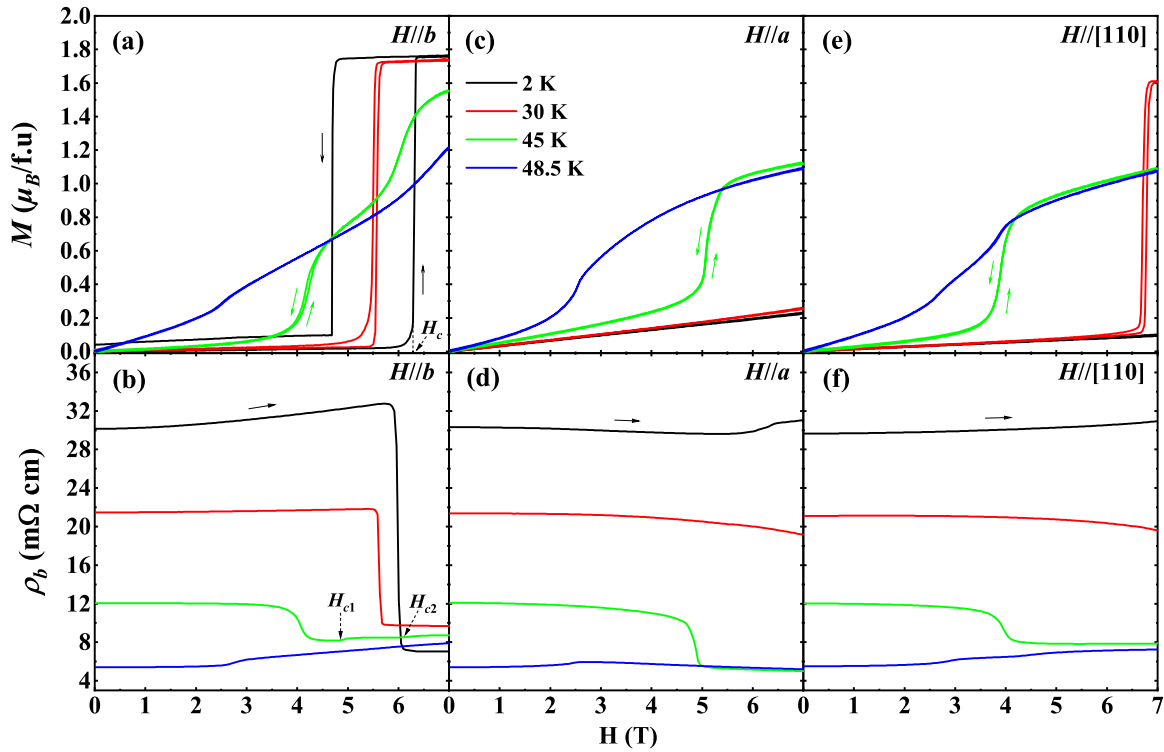


FIG. 2. Magnetic field dependence of magnetization and in-plane resistivity measured under static magnetic field. (a) and (b) For $H\parallel b$, (c) and (d) for $H\parallel a$, (e) and (f) for $H\parallel[110]$. The solid arrows represent the field sweep directions.

resistance hysteresis loop becomes narrow, which disappears at $\theta = 90^\circ$; this is consistent with the second-order phase transition when $H\parallel a$. When $\theta > 29.5^\circ$, the steps appear, and the steps become unrecognizable when $\theta > 58^\circ$ and finally

vanish at $\theta = 90^\circ$, accompanied by the narrowing of the resistance hysteresis loop.

Moreover, no resistance steps were observed under static magnetic field as shown in the inset in Fig. 4(a); thus the resistance steps might be related to the field sweep rate. As displayed in Fig. 4(a), the influence of the field sweep rate on the steps was determined, in which the average sweep rate around the phase transition field changes from 158.46 to 314.87 T/s. However, no significant field sweep rate dependence was observed; this may be because this multistep switching is governed by the inhomogeneous energy landscape, which dominates over the field sweep rate dependence. Overall, this intriguing phenomenon may stem from a rapid dynamic response process, which requires a fast field sweep rate to reveal it. As depicted in Fig. 4(b), the multistep behavior is strongly temperature dependent; that is, the lower the temperature, the greater the number of steps, which almost disappear when $T \geq 3$ K. The results show that the multistep behavior is sensitive to slight thermal fluctuations. Another intriguing aspect is the asymmetry in the variation of ρ_b between the field-ascending and field-descending branches. As shown in Figs. 3 and 4, the multistep variation is clearer in the field-descending branch, signifying the relaxation features, which may suggest the emergence of metastable states during relaxation. Interestingly, this multistep behavior was only observed in the low-temperature region, and no multistep change was observed in magnetization measurements. It seems that this exotic behavior is triggered by other degrees of freedom below a critical temperature. Thus, in spite of the strong spin-charge coupling, we assume that other degrees of freedom, such as lattice and orbital, should be taken into account.

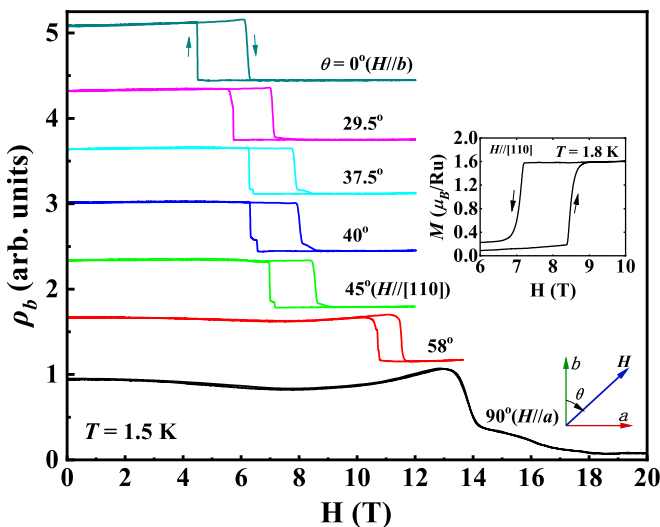


FIG. 3. Magnetic field dependence of the in-plane resistivity with the field direction changing from the b axis to the a axis under pulsed magnetic field. The symbol θ represents the included angle between the b axis and the magnetic field direction. The upper inset shows a local zoom of the magnetization curve at $\theta = 45^\circ$ under pulsed magnetic field, which shows no multistep change.

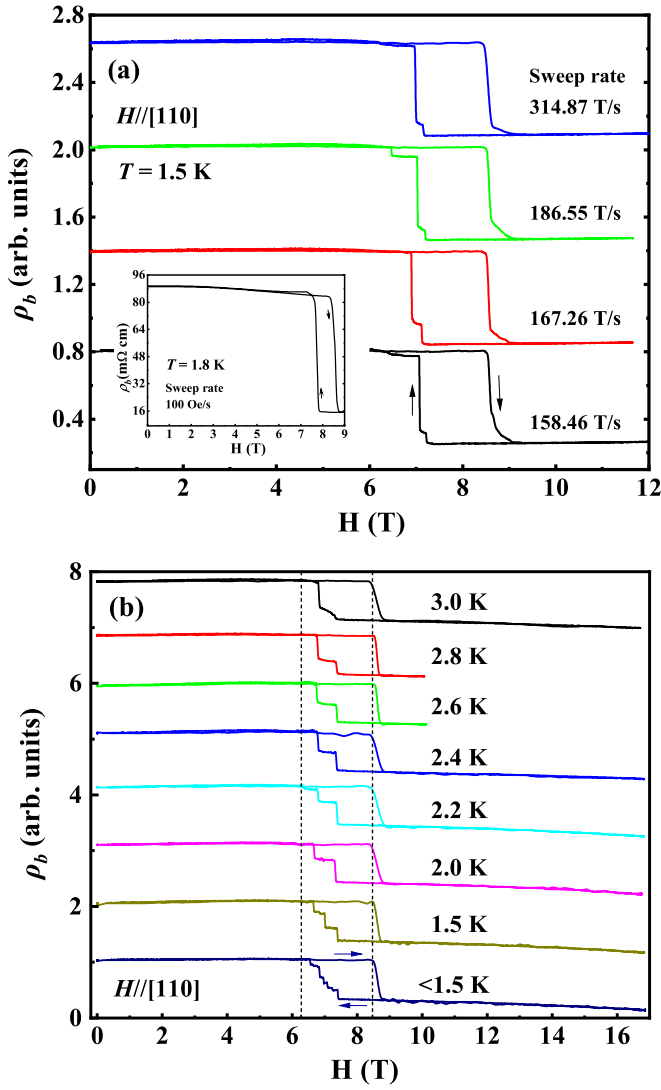


FIG. 4. (a) Magnetic field dependence of in-plane resistivity for $H//[110]$ measured at different field sweep rates under pulsed magnetic field; here the field sweep rate is the average sweep rate around the phase transition field. The inset shows the result under static magnetic field. (b) Magnetic field dependence of in-plane resistivity in the low-temperature region with $H//[110]$.

Figure 5 shows the magnetostriction effect measured under pulsed magnetic field. The negative values of $\Delta L/L$ for the a and b axis signify that both the a axis and the b axis contract, that is, the ab plane is shrunken. The narrow window of the magnetostriction (the sudden change in and recovery of $\Delta L/L$) demonstrates that the structural change is a rapid relaxation process, the lifetime of which is short (approximately milliseconds). The structural change, which was not observed under static magnetic field, also exhibits strong temperature dependence [40], which is consistent with the result presented in Fig. 4(b). In addition, the $\Delta L/L$ decreases as the magnetic field shifts from the b axis to the a axis, indicating that the $\Delta L/L$ is also field direction dependent. Surprisingly, as displayed in Fig. 5(a), this structural change is concomitant with the first-order metamagnetic transition shown in Fig. 2(a),

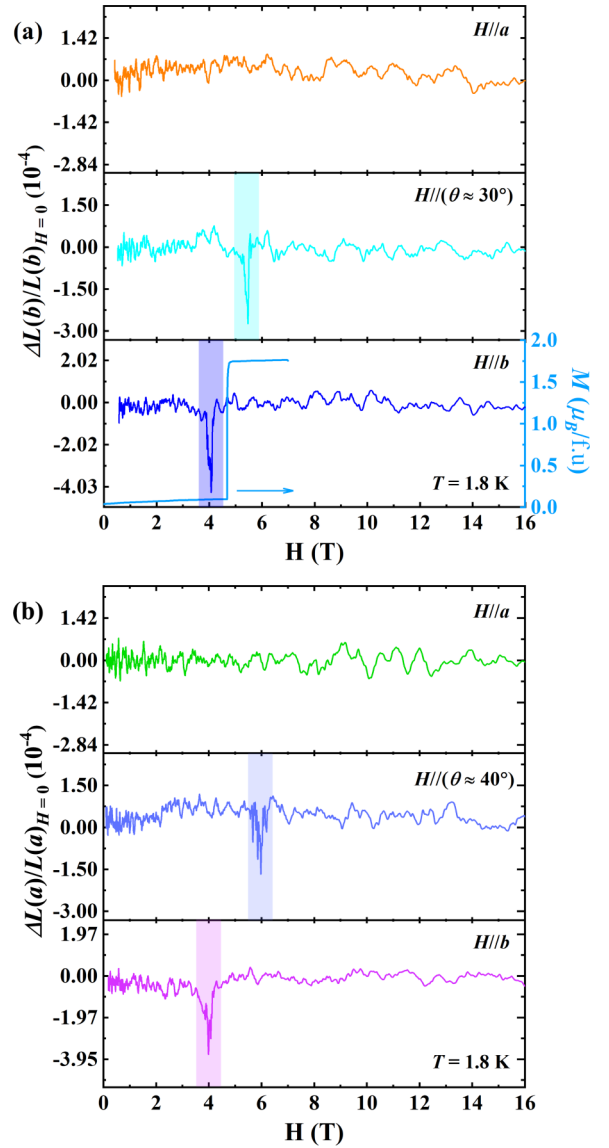


FIG. 5. Magnetostriction measurements for (a) the b axis and (b) the a axis under pulsed magnetic field with an average sweep rate of ~ 300 T/s. Only the results in the field-descending branch are shown here. The magnetization for $H//b$ shown in (a) indicates that the structural change is consistent with the metamagnetic transition.

manifesting the coupling of spin and lattice degrees of freedom.

Metastable states often emerge during the phase transformation to the thermodynamic equilibrium states, which usually have an extended lifetime and can be created via different routes, for instance, by means of rapid cooling, or in phase transitions occurring at low temperature such that thermal fluctuations are not sufficiently strong to overcome the intervening energy barriers in the free-energy landscape. In the latter case the kinetics of the phase transition is arrested, and thus rapid cooling is not necessary [41]. In $\text{Ca}_3\text{Ru}_2\text{O}_7$, the observed multistep behavior occurs in the phase transition regime at low temperature, which may suggest the existence of potential metastable states. For the field-ascending branch, the rapid increase in the magnetic field strongly suppresses

TABLE I. Calculated energies (per 48-atom supercell) of different magnetic states.

State	AFM- <i>b</i>	AFM- <i>a</i>	FM- <i>b</i>	FM- <i>a</i>	Flop	(1/4) Flop
E (meV)	0	38	~ 2	42	13	3.2

the emergence of metastable states. However, in the field-descending branch, when the magnetic field is not along the b axis ($\theta > 0^\circ$), the spin relaxation may lead to some of the spins of the Ru ions pointing towards the a axis, in which situation the metastable states might appear. This may be supported by a previous study in which transverse magnetization measurements revealed the presence of a flop state as shown in Fig. 1, that is, half of the spins of the Ru-O bilayers are aligned along the b axis, while the other half are aligned along the a axis [13].

To explore the possibility of the existence of the metastable states, we calculated the energies of different magnetic states as listed in Table I. Here we take the energy of the AFM- b state, the ground state, as the criterion. We find that the AFM- a state, which has a larger energy of 38 meV, is indeed not the ground state at low temperature; the rather large energy difference between the AFM- a and AFM- b states also indicates the strong magnetocrystalline anisotropy in $\text{Ca}_3\text{Ru}_2\text{O}_7$. In particular, after the structural optimization, the a and b axes in the AFM- b state are longer than those in the AFM- a state, while the c axis is shorter than that in AFM- a state, which perfectly matches the MIT in $\text{Ca}_3\text{Ru}_2\text{O}_7$ due to the spin reorientation [42,43]. To estimate the strength of the AFM interaction in this system, we calculated the energy of the field-induced FM state for all spins aligned along the b axis (FM- b) and a axis (FM- a). The small energy difference between AFM- b and FM- b states (~ 2 meV) indicates that the AFM interaction is weak in this system; a similar result can be seen from the energy difference between AFM- a and FM- a states (4 meV). These results are consistent with the experimental data. Then we calculated the energy of the so-called flop state [13]; the result shows that the spin configuration is stable but with a ground-state energy of 13 meV, which is much higher than that of the AFM- b state. As we presumed that only a small fraction of the spins may point towards the a axis during relaxation, we reduced the proportion of the a -axis-oriented spins. Without loss of generality, the ground-state energy of the $(1/m, m=4)$ flop state (1/4 of the spins of the Ru-O bilayers are aligned along the a axis) was calculated. The result shows that the energy of this state (3.2 meV) is rather smaller than that of the flop state. It can be expected that as m increases, the corresponding energy should get closer to the ground state (AFM- b), indicating that the $(1/m)$ flop state may be a possible intermediate state especially when m is large. Considering the multistep relaxation shown in Figs. 3 and 4, the actual metastable states may also be multiple. That is, the magnetic moments of the Ru-O bilayers pointing towards the a axis continuously relax to the b axis as m gradually increases during relaxation until the ground state is reached. However, despite the consideration of transverse magnetization and metastable states, the temperature dependence of the observed multistep

behavior remains to be explained. Besides, as θ becomes larger, intuitively, there should be more spins pointing towards the a axis during relaxation, and the multistep behavior should be more recognizable; however, the results are the opposite, further implying the involvement of other degrees of freedom.

As presented in Fig. 5, the spin and lattice degrees of freedom are coupled together in $\text{Ca}_3\text{Ru}_2\text{O}_7$. Considering the spin-charge coupling in this system, the multistep magnetoresistance behavior may be the result of the spin-charge-lattice coupling. Typically, the lattice is also coupled to orbital degrees of freedom, which have been reported to play a critical role in determining the magnetoelectric properties of $\text{Ca}_3\text{Ru}_2\text{O}_7$ [15,27,31]. As mentioned before, the MIT in this system is associated with a compression of the Ru-O octahedra, in which the energy of the d_{xy} orbital is lower than that of the d_{yz} and d_{zx} orbitals, which leads to the OO with an approximate d -orbital distribution of $(n_{yz/zx}, n_{xy}) \sim (2, 2)$ via the JT effect below T_{MI} (where $n_{yz/zx}$ is the electron occupancy of the yz and zx orbitals). A comparable situation is also encountered in Ca_2RuO_4 [44]. Therefore it is reasonable to suppose that the rapid structural relaxation may alter the relative energies of the crystal-field-split d levels and the corresponding orbital configurations. We presume that the structural relaxation establishes a dynamic OO-orbital disordering (OD)-OO process: That is, when $\Delta L/L$ is large enough, the d -orbital configuration may be rearranged by increasing $n_{yz/zx}/n_{xy}$ on some of the Ru sites (OO-OD); when $\Delta L/L$ diminishes, as a consequence, the orbital configuration recovers (OD-OO).

Under the above framework, the emergence of the resistance steps can be well understood. When $H \parallel b$ ($\theta = 0^\circ$), the in-plane spin polarization dominates the change in ρ_b , and the system goes through a pure OO-OD-OO process at the phase transition boundary, where no extra resistance steps are observed. As the field direction changes from the b axis to the a axis ($\theta > 0^\circ$), although the $\Delta L/L$ is smaller than that when $H \parallel b$, its intensity is still sufficient to realize the OO-OD-OO process. Meanwhile, in the field-descending branch, the moments having relaxed to the a axis may hinder the system from recovering from the OD state to the OO state via strong spin-orbital interaction. This is supported by Raman scattering studies which show that a mixture of a -axis- and b -axis-oriented moments favors an OD state [27,31]. Consequently, intermediate states with a short lifetime may be established, which are the metastable states discussed during spin relaxation; the process is depicted in Fig. 6. As shown in Fig. 2(b), the two steps marked by H_{c1} and H_{c2} are explained by the OD-to-OO transition due to the electron mobility being more favorable in the OD state [15]. The conductivity (resistivity) of the system should be constant in the metastable states, and the resistance steps appear as a result. However, when θ is small (near 0°), the moments along the a axis during relaxation are small as well, which is insufficient to impact the orbital configurations on the Ru sites, such that the resistance steps are not observed. On the other hand, when θ is large (near 90°), the structural change is rather too weak to realize the OO-OD-OO process, and the resistance steps are also not observed. At higher temperatures, as shown in Fig. S4(a) of the Supplemental Material [40], the structural change is much smaller, so the resistance steps are not observed.

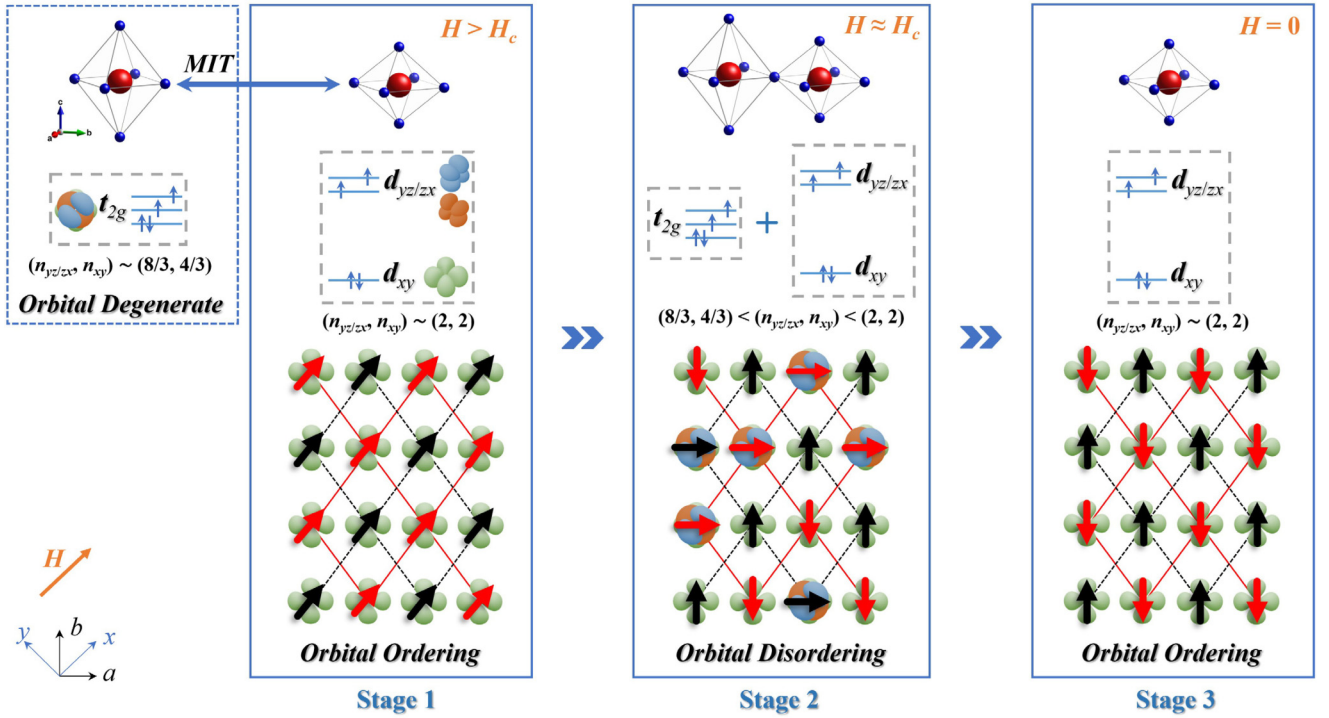


FIG. 6. Here we denote the electron occupancy of the yz and zx orbitals and the electron occupancy of the xy orbital as $n_{yz/zx}$ and n_{xy} , respectively. Before the MIT at $T_{\text{MI}} = 48$ K, the three t_{2g} orbitals are degenerate with an approximate d -orbital distribution of $(n_{yz/zx}, n_{xy}) \sim (8/3, 4/3)$; that is, the four $4d$ electrons of the Ru^{4+} ions evenly occupy the three t_{2g} orbitals, showing a high conducting behavior. After the MIT, the degeneracy of the three t_{2g} orbitals is partly lifted via the JT effect, resulting in the energy of the d_{xy} orbital being lower than that of the d_{yz} and d_{zx} orbitals and two of the four electrons of the Ru^{4+} ions occupying the d_{xy} orbital while another two occupy the d_{yz} and d_{zx} orbitals, which leads to the OO with an approximate d -orbital distribution of $(n_{yz/zx}, n_{xy}) \sim (2, 2)$, showing a low conducting behavior. When $H > H_c$, the spins are polarized to the direction of the external magnetic field, and the orbital pattern is not affected (stage 1). When the strength of the external magnetic field approaches the phase transition boundary during demagnetization ($H \approx H_c$), the contraction of the ab plane (lattice relaxation) reflects the splitting of the t_{2g} levels via the JT effect and the fluctuation of the orbital pattern; that is, the d -orbital distribution on some of the Ru sites is rearranged which increases the average $(n_{yz/zx}, n_{xy})$ to $(8/3, 4/3) < (n_{yz/zx}, n_{xy}) < (2, 2)$. Simultaneously, the spin relaxation on the Ru sites interacts with the orbital via strong spin-orbital interaction, which leads to the emergence of the resistance steps (stage 2). After the spin and lattice relaxation ($H = 0$), the system recovers to the ground state with a d -orbital distribution of $(n_{yz/zx}, n_{xy}) \sim (2, 2)$ (stage 3). The red and black arrows represent the spins of the Ru ions on different Ru-O bilayers; ab and xy represent the crystal and local coordinates, respectively.

Let us now focus on the possible form of the spin-orbital interaction and the nature of the dynamic OO-OD-OO process. According to the Kugel-Khomskii model, the change in the spin configuration can affect the orbital configuration in orbital active systems [2,3]; therefore the magnetic field may alter the orbital state of the Ru sites in $\text{Ca}_3\text{Ru}_2\text{O}_7$. On the other hand, the altering of the orbital state can be reflected through the cooperative JT effect, i.e., the distortion of the lattice. Therefore the observed magnetostriction behavior may be attributed to a field-induced dynamic process resulting from the combination of the two aforementioned mechanisms. Namely, the magnetostriction effect reflects the OO-OD-OO process arising from a transient Kugel-Khomskii interaction. Furthermore, considering the distinct anisotropy between the b axis and a axis that arises from the strong SOC in this system, the decreasing of $\Delta L/L$ with magnetic field shifts from the b axis to the a axis may be interpreted as the consequence of the competition between the Kugel-Khomskii interaction and the magnetic anisotropy. That is, when $H \parallel b$, the Kugel-Khomskii interaction is dominant, and the resultant magnetostriction effect is significant; when $H \parallel a$, the mag-

netic anisotropy is primary, which strongly suppresses the Kugel-Khomskii interaction, such that the magnetostriction effect is not observed. Last but not least, the Kugel-Khomskii interaction may be rather weak in $\text{Ca}_3\text{Ru}_2\text{O}_7$, where the multistep magnetoresistance behavior and the magnetostriction effect are only observable in the low-temperature region [40]. This may be related to the weak spin-orbital interactions in the t_{2g} orbitals of the Ru ions, the strength of which is weaker than that in the e_g orbitals.

IV. CONCLUSION

In summary, this work unveils the existence of instantaneous interactions between spin, charge, orbital, and lattice degrees of freedom in the $4d$ correlated electronic system of $\text{Ca}_3\text{Ru}_2\text{O}_7$, and the phenomena resulting from these interactions can be observed under pulsed magnetic field owing to its fast field sweep rate. Specifically, a multi-step magnetoresistance behavior was observed under pulsed magnetic field in a $\text{Ca}_3\text{Ru}_2\text{O}_7$ single crystal, which is accompanied by a field-induced structural change. In particular,

no multistep magnetoresistance behavior was observed under static magnetic field, and no multistep change was observed in the magnetization measurements. We propose that the appearance of the resistance steps is due to the metastable states induced by transient Kugel-Khomskii-type spin-orbital interactions during spin relaxation (in the field-descending branch). That is, while the structural change realizes an OO-OD-OO process by distorting the Ru-O octahedra, the resistance steps are induced by establishing metastable states via transient Kugel-Khomskii-type spin-orbital interactions during the OO-OD-OO process. Furthermore, this transient Kugel-Khomskii interaction can be strongly suppressed by

the magnetocrystalline anisotropy. This study may provide insight to understand the dynamic characteristics in systems which host complicated interactions between multiple degrees of freedom, especially in those with t_{2g} active orbital degrees of freedom.

ACKNOWLEDGMENTS

This work is supported in part by the National Natural Science Foundation of China (Grants No. 11674115 and No. 51861135104). We are sincerely thankful to Prof. G. Cao for providing the single-crystal samples.

-
- [1] G. Binasch, P. Grünberg, F. Saurenbach, and W. Zinn, *Phys. Rev. B* **39**, 4828 (1989).
- [2] K. I. Kugel' and D. I. Khomskii, *Zh. Eksp. Teor. Fiz.* **64**, 1429 (1973) [*Sov. Phys.-JETP* **37**, 725 (1973)].
- [3] K. I. Kugel and D. I. Khomskii, *Sov. Phys.-Usp.* **25**, 231 (1982).
- [4] J. B. Goodenough, *Phys. Rev.* **100**, 564 (1955).
- [5] S. Kunkemöller, D. Brüning, A. Stunault, A. A. Nugroho, T. Lorenz, and M. Braden, *Phys. Rev. B* **96**, 220406(R) (2017).
- [6] Y. Shirako, H. Satsukawa, X. X. Wang, J. J. Li, Y. F. Guo, M. Arai, K. Yamaura, M. Yoshida, H. Kojitani, T. Katsumata, Y. Inaguma, K. Hiraki, T. Takahashi, and M. Akaogi, *Phys. Rev. B* **83**, 174411 (2011).
- [7] A. P. Mackenzie, R. K. W. Haselwimmer, A. W. Tyler, G. G. Lonzarich, Y. Mori, S. Nishizaki, and Y. Maeno, *Phys. Rev. Lett.* **80**, 161 (1998).
- [8] T. Mizokawa, L. H. Tjeng, G. A. Sawatzky, G. Ghiringhelli, O. Tjernberg, N. B. Brookes, H. Fukazawa, S. Nakatsuji, and Y. Maeno, *Phys. Rev. Lett.* **87**, 077202 (2001).
- [9] I. Zegkinoglou, J. Stempfer, C. S. Nelson, J. P. Hill, J. Chakhalian, C. Bernhard, J. C. Lang, G. Srajer, H. Fukazawa, S. Nakatsuji, Y. Maeno, and B. Keimer, *Phys. Rev. Lett.* **95**, 136401 (2005).
- [10] S. Raghu, A. Paramekanti, E.-A. Kim, R. A. Borzi, S. A. Grigera, A. P. Mackenzie, and S. A. Kivelson, *Phys. Rev. B* **79**, 214402 (2009).
- [11] Y. Yoshida, S.-I. Ikeda, H. Matsuhata, N. Shirakawa, C. H. Lee, and S. Katano, *Phys. Rev. B* **72**, 054412 (2005).
- [12] W. Bao, Z. Q. Mao, Z. Qu, and J. W. Lynn, *Phys. Rev. Lett.* **100**, 247203 (2008).
- [13] S. McCall, G. Cao, and J. E. Crow, *Phys. Rev. B* **67**, 094427 (2003).
- [14] H. Xing, L. Wen, C. Shen, J. He, X. Cai, J. Peng, S. Wang, M. Tian, Z.-A. Xu, W. Ku, Z. Mao, and Y. Liu, *Phys. Rev. B* **97**, 041113(R) (2018).
- [15] X. N. Lin, Z. X. Zhou, V. Durairaj, P. Schlottmann, and G. Cao, *Phys. Rev. Lett.* **95**, 017203 (2005).
- [16] C. S. Nelson, H. Mo, B. Bohnenbuck, J. Stempfer, N. Kikugawa, S. I. Ikeda, and Y. Yoshida, *Phys. Rev. B* **75**, 212403 (2007).
- [17] S. V. Streltsov and D. I. Khomskii, *Phys.-Usp.* **60**, 1121 (2017).
- [18] Y. Tokura and N. Nagaosa, *Science* **288**, 462 (2000).
- [19] H.-Y. Niu, Z. Zeng, Y.-J. Song, H. Huang, Y.-Y. Liang, D.-Q. Jiang, Z.-M. Tian, Z.-W. Ouyang, and Z.-C. Xia, *Phys. Rev. B* **105**, 054401 (2022).
- [20] S. Lei, M. Gu, D. Puggioni, G. Stone, J. Peng, J. Ge, Y. Wang, B. Wang, Y. Yuan, K. Wang, Z. Mao, J. M. Rondinelli, and V. Gopalan, *Nano Lett.* **18**, 3088 (2018).
- [21] H. L. Liu, S. Yoon, S. L. Cooper, G. Cao, and J. E. Crow, *Phys. Rev. B* **60**, R6980 (1999).
- [22] G. Cao, K. Abbound, S. McCall, J. E. Crow, and R. P. Guertin, *Phys. Rev. B* **62**, 998 (2000).
- [23] G. Cao, L. Balicas, Y. Xin, E. Dagotto, J. E. Crow, C. S. Nelson, and D. F. Agterberg, *Phys. Rev. B* **67**, 060406(R) (2003).
- [24] G. Cao, L. Balicas, Y. Xin, J. E. Crow, and C. S. Nelson, *Phys. Rev. B* **67**, 184405 (2003).
- [25] G. Cao, L. Balicas, X. N. Lin, S. Chikara, E. Elhami, V. Duairaj, J. W. Brill, R. C. Rai, and J. E. Crow, *Phys. Rev. B* **69**, 014404 (2004).
- [26] E. Ohmichi, Y. Yoshida, S. I. Ikeda, N. Shirakawa, and T. Osada, *Phys. Rev. B* **70**, 104414 (2004).
- [27] J. F. Karpus, C. S. Snow, R. Gupta, H. Barath, S. L. Cooper, and G. Cao, *Phys. Rev. B* **73**, 134407 (2006).
- [28] G. Cao, S. McCall, J. E. Crow, and R. P. Guertin, *Phys. Rev. Lett.* **78**, 1751 (1997).
- [29] A. V. Puchkov, M. C. Schabel, D. N. Basov, T. Startseva, G. Cao, T. Timusk, and Z.-X. Shen, *Phys. Rev. Lett.* **81**, 2747 (1998).
- [30] C. S. Snow, S. L. Cooper, G. Cao, J. E. Crow, H. Fukazawa, S. Nakatsuji, and Y. Maeno, *Phys. Rev. Lett.* **89**, 226401 (2002).
- [31] J. F. Karpus, R. Gupta, H. Barath, S. L. Cooper, and G. Cao, *Phys. Rev. Lett.* **93**, 167205 (2004).
- [32] D. J. Singh and S. Auluck, *Phys. Rev. Lett.* **96**, 097203 (2006).
- [33] F. Baumberger, N. J. C. Ingle, N. Kikugawa, M. A. Hossain, W. Meevasana, R. S. Perry, K. M. Shen, D. H. Lu, A. Damascelli, A. Rost, A. P. Mackenzie, Z. Hussain, and Z.-X. Shen, *Phys. Rev. Lett.* **96**, 107601 (2006).
- [34] D. Fobes, J. Peng, Z. Qu, T. J. Liu, and Z. Q. Mao, *Phys. Rev. B* **84**, 014406 (2011).
- [35] H. Zhao, H. Zheng, J. Terzic, W. Song, Y. Ni, Y. Zhang, P. Schlottmann, and G. Cao, *Phys. Rev. B* **104**, L121119 (2021).
- [36] G. Kresse and D. Joubert, *Phys. Rev. B* **59**, 1758 (1999).
- [37] J. P. Perdew, A. Ruzsinszky, G. I. Csonka, O. A. Vydrov, G. E. Scuseria, L. A. Constantin, X. Zhou, and K. Burke, *Phys. Rev. Lett.* **100**, 136406 (2008).
- [38] G. Kresse and J. Furthmüller, *Phys. Rev. B* **54**, 11169 (1996).
- [39] P. E. Blöchl, *Phys. Rev. B* **50**, 17953 (1994).
- [40] See Supplemental Material at <http://link.aps.org/supplemental/10.1103/PhysRevB.106.174415> for detailed magnetization, magnetoresistance, and temperature-dependent magnetostric-

- tion measurements for different field directions and crystalline axes, which includes Refs. [14,15,34].
- [41] P. G. Debenedetti and F. H. Stillinger, *Nature (London)* **410**, 259 (2001).
- [42] Y. Yuan, P. Kissin, D. Puggioni, K. Cremin, S. Lei, Y. Wang, Z. Mao, J. M. Rondinelli, R. D. Averitt, and V. Gopalan, *Phys. Rev. B* **99**, 155111 (2019).
- [43] I. Marković, M. D. Watson, O. J. Clark, F. Mazzola, E. A. Morales, C. A. Hooley, H. Rosner, C. M. Polley, T. Balasubramanian, S. Mukherjee, N. Kikugawa, D. A. Sokolov, A. P. Mackenzie, and P. D. C. King, *Proc. Natl. Acad. Sci. U. S. A.* **117**, 15524 (2020).
- [44] J. S. Lee, Y. S. Lee, T. W. Noh, S.-J. Oh, J. Yu, S. Nakatsuji, H. Fukazawa, and Y. Maeno, *Phys. Rev. Lett.* **89**, 257402 (2002).